Charge Transport in Organometal Halide Perovskites

Francesco Maddalena, Pablo P. Boix, Chin Xin Yu, Nripan Mathews, Cesare Soci and Subodh Mhaisalkar

1 Introduction

One of the most important features in any semiconductor device is the charge transport of the active materials. The charge transport mode and the effective charge mobility strongly determine whether a material is suitable for a particular application. A clear example is the relative low mobility of organic semiconductors, compared to their crystalline inorganic counterparts, which makes organic semiconductors unsuitable for high-end electronic applications. Moreover, a deep understanding of the charge transport properties of a particular set of materials is essential for the development of new device architectures and the improvement of the available technological applications.

Recently, the use of organometal halide perovskites, in particular $CH_3NH_3PbI_3$, has generated very promising results in the fabrication of efficient low-cost solar cells. Figure 1 shows how the efficiency of perovskite solar cells has rapidly increased in the last 5 years, surpassing most of its "low cost" competitors and reaching efficiencies exceeding 21 % [1], with their excellent charge transport characteristics underpinning their success. Being solution processable, hybrid perovskites offer advantages similar to organic semiconductors in terms of device fabrication and up-scalability. Moreover, hybrid perovskites have shown great

F. Maddalena · P.P. Boix · N. Mathews · S. Mhaisalkar (✉)
Energy Research Institute @ NTU (ERI@N), Research Technoplaza,
Nanyang Technological University, Nanyang Drive, Singapore 637553, Singapore
e-mail: Subodh@ntu.edu.sg

F. Maddalena · C. Xin Yu · C. Soci
Division of Physics and Applied Physics, Nanyang Technological University,
Singapore 637371, Singapore

N. Mathews · S. Mhaisalkar
School of Materials Science and Engineering, Nanyang Technological University,
Nanyang Avenue, Singapore 639798, Singapore

N.-G. Park et al. (eds.), *Organic-Inorganic Halide Perovskite Photovoltaics*,
DOI 10.1007/978-3-319-35114-8_8

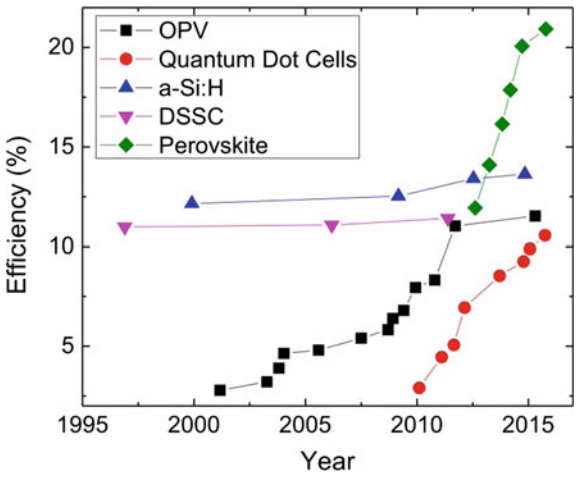

Fig. 1 Evolution of the efficiency of solution-processed perovskite solar cells compared to organic photovolatic (OPV), quantum dot, dye-sensitized (DSSC), and amorphous hydrogenated silicon (a-Si:H) solar cells. Adapted and printed with permission from the National Center for Photovoltaics at NREL solar cell efficiency chart. Reprinted with permission of the National Renewable Energy Laboratory, from http://www.nrel.gov/ncpv/images/efficiency_chart.jpg. Accessed February 12th, 2016

versatility in terms of tunability and efficiency of optoelectronic properties by chemical routes, making them ideal candidates for applications in electroluminescent devices, lasing [2], light-detectors, and thermoelectric energy conversion. Solution-processed perovskite LEDs have already shown very high electroluminescence efficiency and even light-emitting FETs have been reported [3].

In this chapter, we review the theoretical models and experimental observations regarding charge transport in hybrid perovskites available to date, in particular for methylammonium lead iodide and methylammonium lead mixed-halide perovskites, which are currently the most widely studied materials of this class. We will first look at the results from theoretical ab initio calculations of organometallic perovskites, showing potential for very high mobility and efficient charge transport. Then, we shall look at the experimental determination of the diffusion length of charge carriers in organometallic perovskites. Very long diffusion lengths, exceeding the micrometer scale have been experimentally deduced in solution-processed perovskite films and single crystals, making them extremely appealing for various semiconductors applications. Field-effect charge carrier mobilities will then be discussed, which are found to be much lower than the theoretical estimates and the experimental values determined by Hall-effect measurements. Effects of ionic motion and possible ferroelectric effects seem to be responsible for the low performance in FETs and for the large hysteresis and low stability of most organometallic perovskite devices. To conclude, we will give some perspectives on the transport characteristics of emerging two-dimensional (2D) perovskites as well as lead-free compounds, which are attractive alternatives from a commercial and environmental point of view.

2 Theoretical Studies on Charge Transport in Hybrid Perovskites

Following the promising initial results in hybrid perovskite photovoltaics, theoretical studies have been conducted to investigate charge transport characteristics of this class of materials. Ab initio calculations have been performed on models of $CH_3NH_3MI_3$ perovskites (M = Sn, Pb), based on Density Functional Theory (DFT) and many body perturbation theory (MBPT), while approximate models were used to estimate the charge carrier density in the material. The predicted band structure and density of stated (DoS) resulting from the ab initio calculations are shown in Fig. 2.

The investigation of three configurations of $CH_3NH_3PbI_3$, with the dipole of the methylammonium cation along three different orientations ((100), (110), and (111) crystal directions), can help to mimic the disorder in polycrystalline perovskite films. Although the change in the organic cation orientation has noticeable effects on the computed lattice constants, the final calculated energy difference was found to be relatively small between the calculated configurations, within 40 meV. This fact helps explaining the discrepancies between experimental studies [6, 7], where samples may contain different orientations of the organic cations, leading to some variability in the results, as experimentally synthesized perovskites are expected to have lattice constants with values averaged over the all possible configurations. The predicted band structures of the $CH_3NH_3MI_3$ perovskites reveal a quasi-direct bandgap at the R symmetry point of the Brioullin zone, for both the lead and the tin variants. Calculated values of the gaps are 1.36 eV and 1.51 eV for Pb and Sn respectively [16], relatively close to the experimentally determined values of 1.57 eV and 1.20 eV respectively for Pb and Sn [8, 9]

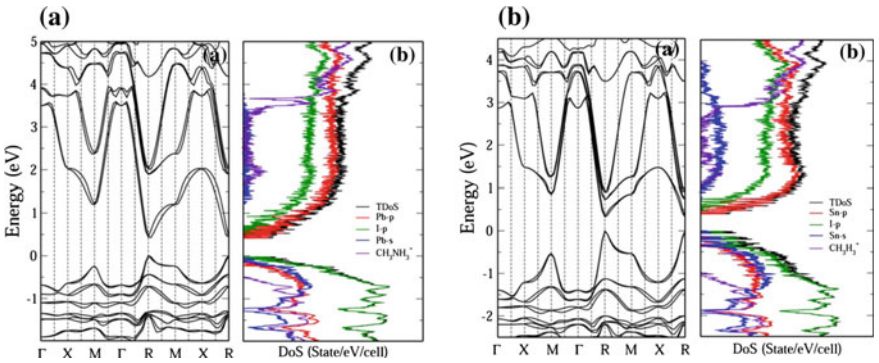

Fig. 2 Band structure (*left panel*) calculated from density functional theory and density of states (DoS) (*right panel*) of methylammonium lead iodide (**a**) and methylammonium tin iodide (**b**). The band structure shown assumes the dipole of $CH_3NH_3^+$ along the (100) direction. The total DoS (TDoS, *black*) is shown along with the partial electronic density of states (DoS) contributions from the metal (Pb or Sn) p-orbitals (*red*), I-p-orbtials (*green*), the metal (Pb or Sn) s-orbitals (*blue*), and the organic cation (*purple*). Adapted and printed with permission from [5]

Theoretical calculations predict very high theoretical mobilities: μ_e = 3100–1500 $cm^2/V\ s$ and μ_h = 500–800 $cm^2/V\ s$ for the lead-based perovskite and μ_e = 2700–1300 $cm^2/V\ s$ and μ_h = 3100–1400 $cm^2/V\ s$ for the tin-based perovskites at charge carrier concentrations of $\sim 10^{16}\ cm^{-3}$. These values, very high compared to other hybrid or organic semiconductors, are of the same order of magnitude of crystalline inorganic semiconductors such as silicon or gallium arsenide.

Calculations have shown that the large carrier mobilities mainly originate from a combination of two factors. First, the small effective masses m^* of electrons and holes (Table 1), with the DoS effective mass being, on average, 0.2333 m_0 and 0.2583 m_0 (m_0 being the rest mass of the electron) for the lead-based perovskite, and 0.3040 m_0 and 0.1906 m_0 for the tin-based perovskite. Such low effective masses were confirmed experimentally through magneto-absorption measurements [10]. The second factor is the relatively weak carrier–phonon interaction, in the range of 6.5–10 eV for both analyzed perovskite materials. The weak electron–phonon coupling is also consistent with the large diffusion lengths determined experimentally for the charge carriers [11–14].

Similar results and conclusions have been reached also by Giorgi et al. [13], which also showed comparably low values for the effective mass of charge carriers (>0.3 m_0) for the methylammonium lead iodide perovskite.

The effective mass and temperature-dependent mobility for two different crystalline phases of $MAPbI_3$, orthorhombic (below T = 160 K), and tetragonal (above T = 160 K) show slightly better conductivity for electrons than holes, as shown in Fig. 3. Low effective masses are predicted, close to the values reported above, with slightly larger values for the orthorhombic phase and overall larger hole effective masses, consistent with lower predicted hole mobilities (tetragonal: m_e^* = 0.197 m_0, m_h^* = 0.340 m_0, orthorhombic: m_e^* = 0.239 m_0, m_h^* = 0.357 m_0). Within the investigated temperature range (78–300 K), electron mobilities exceed hole mobilities by approximately a factor of two, and an increase by nearly one order of magnitude, for both electron and hole mobilities, is predicted below the phase transition temperature (μ_e = 2,577–11,249 $cm^2\ V^{-1}\ s^{-1}$ and μ_h = 1,060–4,630 $cm^2\ V^{-1}\ s^{-1}$ for the orthorhombic phase and μ_e = 466–2,046 $cm^2\ V^{-1}\ s^{-1}$ and μ_h = 140–614 $cm^2\ V^{-1}\ s^{-1}$ for the tetragonal phase).

Experimental determination of the mobility in perovskites by different methods has reflected these high theoretical values. Combining resistivity and Hall-effect

Table 1 Average values of the longitudinal ($m_\parallel^*$), transverse ($m_\perp^*$), conductivity (m_C^*), band (m_b^*) and density of states (m^*), effective mass for electrons (e^-) and holes (h^+) in $MAPbI_3$ and $MASnI_3$

	$MAPbI_3\ e^-$	$MAPbI_3\ h^+$	$MASnI_3\ e^-$	$MASnI_3\ h^+$
$m_\parallel^*$	0.2095	0.3060	0.3332	0.1540
$m_\perp^*$	0.0881	0.0840	0.1027	0.0750
m_I^*	0.1081	0.1107	0.1334	0.0904
m_b^*	0.1166	0.1291	0.1520	0.9530
m^*	0.2333	0.2583	0.3040	0.1906

Adapted and printed with permission from [5]

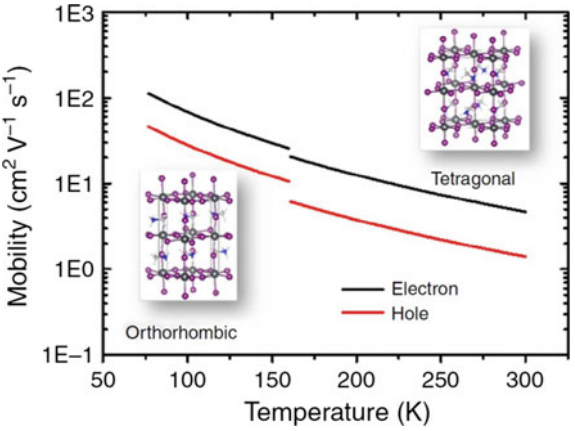

Fig. 3 Calculated temperature dependence hole (*red curves*) and electron (*black curves*) mobility in tetragonal (T = 300–160 K) and orthorhombic (T = 160–77 K) phases of $CH_3NH_3PbI_3$. The crystal unit cells of the two phases are shown as insets. Adapted and printed with permission from [4]

measurements, electron mobilities of $\sim$2320 cm^2/V s in $CH_3NH_3SnI_3$ have been measured [9]. However, for $CH_3NH_3PbI_3$, the experimental mobilities determined by Hall-effect measurements were only of the order of 66 cm^2/V s, significantly lower than the theoretical calculations, although an order of magnitude higher than other solution-processed materials [9, 15].

The influence of the cations and the (halide) anions on the bandgap energy of solution-processed perovskites has been investigated through density functional theory as well [16]. An overview is shown in Fig. 4. The calculations indicate that the bandgap of a perovskite with Orthorhombic structure is distinctively larger than

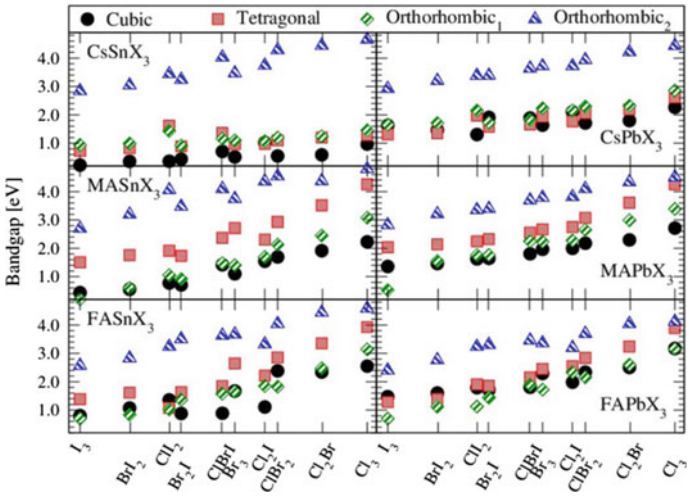

Fig. 4 Theoretically calculated bandgaps as a function of the electronegativity of the anions for different crystalline structures of lead- and tin-based perovskites with different cations are shown: Cesium (Cs), methylammonium (MA) and formamidinium (FA). Adapted and printed with permission from [16]

other crystal structures (cubic, tetragonal). In general, with some exceptions, increasing the tilt of the structure, from cubic to orthorhombic, also leads to an increase of the bandgap. The increase in electronegativity in the anion, ranging from the least electronegative triiodide variant to the most electronegative trichloride, corresponds with a quasilinear increase in the bandgap energy. This trend has been partially confirmed experimentally [8, 9, 17]. The influence of the cations strongly affects the bandgap as well. Increasing the volume of the cation, going from the smallest (Cesium) to the largest (formamidinium) has the effect of increasing the volume of the perovskite unit cell and lattice constants, corresponding to an increase of the bandgap of the material. These results show the tunability and versatility of solution-processable perovskites, especially suitable for optoelectronic applications. The general trends predicted by theoretical calculations, and reflected in current experimental observations, are the basis for the development of novel hybrid perovskites.

3 Charge Carrier Diffusion Length in Hybrid Perovskites

Long electron and hole diffusion lengths, preferably greater than 100 nm, are critical for the development of highly efficient solar cells and junction devices. Large diffusion lengths are responsible for the relatively high efficiencies of solar cells based on classical inorganic semiconductors, like silicon, since they favor electron-hole separation and reduce recombination losses. Polycrystalline organolead trihalide perovskites, such as $CH_3NH_3PbI_3$, have shown very long diffusion lengths, to which was partly attributed the high efficiency of solution-processed solar cells.

Several studies [11–14] have shown that the diffusion lengths for electron and holes in polycrystalline, solution-processed $CH_3NH_3PbI_3$ exceed 100 nm. Such diffusion lengths are at least an order of magnitude larger than those of most organic solution-processed materials (such as P3HT-PCBM bulk heterojunctions), in which diffusion lengths are typically lower than 10 nm [18–20], and are responsible for the high recombination rates.

In good agreement, transient absorption and photoluminescence-quenching measurements determining the electron-hole diffusion lengths in halide perovskites showed balanced diffusion lengths of over 100 nm for both electrons and holes in the triiodide perovskite and, notably, diffusion length of over 1 μm were also reported in the mixed halide variant [11]. Measurements in solar cells showed that the increased diffusion length correlates with an increase in efficiency of photovoltaic devices: from 4.2 to 12.2 % in planar heterojunction solar cells fabricated with the triiodide and the mixed halide perovskite, respectively. Currently, the mechanism that causes the increase of electron-hole diffusion length upon addition of small quantities of chloride ions during the fabrication of $CH_3NH_3PbI_3$, inhibiting nonradiative exciton recombination, is not fully understood. However, it seems to be directly related to film crystallization rather than to material doping [21, 22].

Large charge carrier diffusion lengths for $CH_3NH_3PbI_3$ were also obtained by femtosecond transient optical spectroscopy measurements of bilayers consisting in perovskites with either selective-electron or selective-hole extraction materials (Fig. 5) [12].

Studies on single crystal methylammonium lead iodide have shown diffusion lengths that greatly exceed solution-processed films. Diffusion lengths of over 175 μm under one-sun illumination and diffusion lengths exceeding 3 mm under weak illumination (0.003 % sun) have been observed in solution-grown $CH_3NH_3PbI_3$ single crystals [14]. The enhanced diffusion lengths in single crystals is understood as a combination of greater carrier mobility, longer lifetime, and much smaller trap densities in the single crystals than in polycrystalline thin films. These result from the absence of structural and grain boundary defects that are present in polycrystalline films, indicating possible strategies to improve the electrical properties of perovskite-based devices.

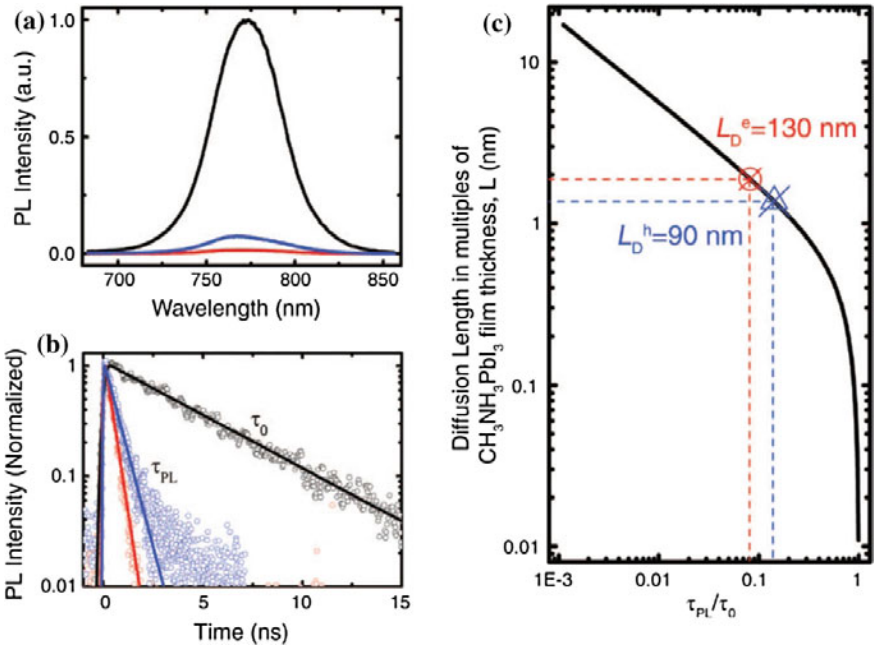

Fig. 5 **a** Time-integrated PL spectra and **b** Time-resolved PL decay transients for quartz/$CH_3NH_3PbI_3$ (*black*), quartz/$CH_3NH_3PbI_3$ (65 nm)/PCBM (*red*), quartz/$CH_3NH_3PbI_3$ (65 nm)/Spiro-OMeTAD (*blue*) films in vacuum after excitation at 600 nm. The *solid lines* in (**b**) are the single-exponential fits of the PL decay transients. **c** A plot of exciton diffusion length versus PL lifetime quenching ratios. Diffusion length is scaled in multiples of $CH_3NH_3PbI_3$ layer thickness (L = 65 nm). Adapted and printed with permission from [12]

4 Charge Carrier Mobility in FET and LED Devices

Although theoretical mobilities in hybrid perovskites are comparable to those of crystalline inorganic semiconductors, and Hall-effect measurements yield very high values, the effective carrier mobility in field-effect transistors (FETs) and diodes is much lower than expected. Peak values for the field-effect mobility in perovskite transistors showed values of the order of 0.5 cm^2/V s for both solution-processed three-dimensional (3D) [4] and 2D-layered perovskites [23]. Several different compositions of organometallic halide perovskites have been investigated in FET configurations, varying the organic cation, the metal cation, or the halide anion. The measured mobilities at saturation fall between 0.01 and 0.1 cm^2/V s, while linear mobilities are usually an order of magnitude lower [24]. Mobilities above 1 cm^2/V s were achieved in melt-processed tin-based organometallic perovskites, where the perovskite films were heated ~5 °C above the melting point and then allowed to recrystallize [25]. Phototransistors showed also mobilities above 0.1 cm^2/V s when the FETs where exposed to white light (10 mW cm^{-2}) [26].

Thus, despite their potential, the best effective mobilities of perovskite FETs are in the same range of state-of-the-art, solution-processed polymer semiconductor FETs (e.g.: N2200, 0.1–1 cm^2/V s for electrons [27]; PBTTT > 0.1 cm^2/V s for holes, [28]). Moreover, since the charge carrier concentration in LED is usually several orders of magnitude lower than in FETs, the low effective charge carrier mobility of solution-processed perovskites presents even more severe problems for the realization of efficient charge injection, charge transport and electroluminescence in light-emitting diodes.

Current studies on solution-processed perovskite FETs have also shown a lack of proper transistor behavior at temperatures above ~200 K [4]. Room temperature transfer characteristics of methylammonium halide FETs show a lack of gating behavior, resulting in transfer curves that are independent of the gate voltage, as depicted in the transfer characteristics in Fig. 6a. Lowering the temperature below ~200 K restores the gating effect in the FETs and increases the current by almost three orders of magnitude (Fig. 6b, c). However, even at low temperatures, the transfer and output characteristics exhibit a strong hysteretic behavior (Fig. 6b, c), similar to the one observed in solar cells [29]. The origin of the hysteresis is uncertain, and it is possibly caused by ionic drift, ferroelectric behavior, and/or presence of traps (see Sect. 5). Experimental measurements on the effective charge carrier mobility in hybrid perovskite FETs have shown a strong dependence on temperature, reflecting some of the theoretical predictions discussed in the previous section [4]. At room temperature, $CH_3NH_3PbI_3$ FETs exhibit very low mobilities, in the range of $\sim 10^{-6}$ cm^2/V s, below even most amorphous organic semiconductors. On the other hand, decreasing the temperature below ~200 K, results in a sharp increase of mobility of over five orders of magnitude as shown in Fig. 7. Previously mentioned theoretical calculations by Chin et al., have shown that above 160 K the perovskite has a morphological change (from a tetragonal to orthorhombic structure) which might be a partial cause of the increase in the

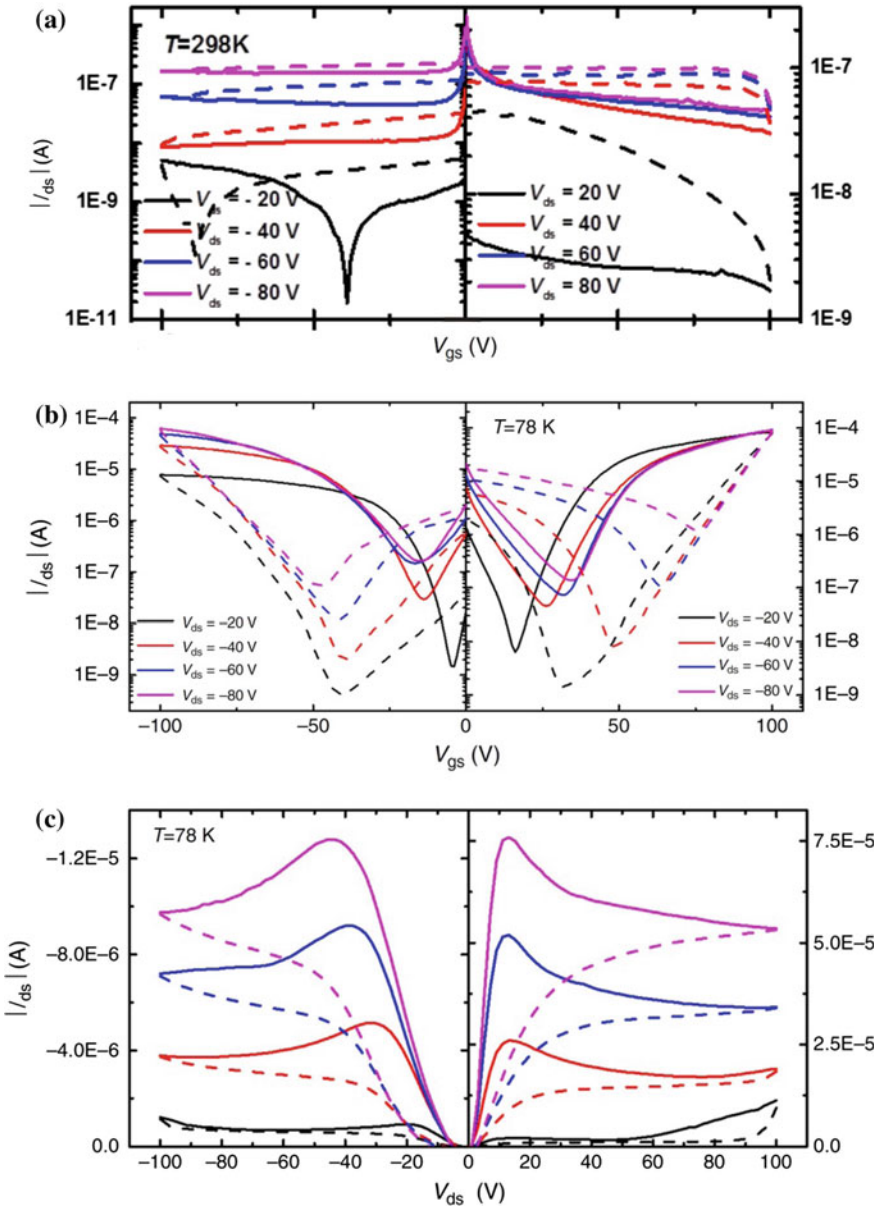

Fig. 6 **a** Transfer characteristics of $CH_3NH_3PbI_3$ FET obtained at 298 K. Transfer (**b**) and output (**c**) characteristics obtained at 78 K. Both the n-type (*right panel*) and p-type (*left panel*) regime. Adapted and printed with permission from [4]

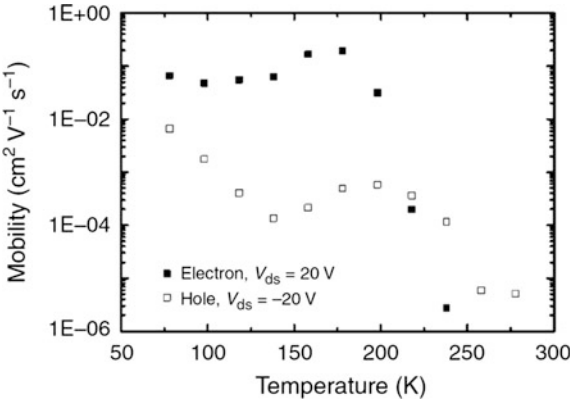

Fig. 7 Temperature dependence of field-effect electron and hole mobilities, extracted from the forward sweeping of transfer characteristics. Adapted and printed with permission from [4]

mobility. However, this phase transition alone is not sufficient to explain the drop in mobility above 180 K, the strong discrepancy between calculated and measured values and the lack of gating at room temperature. The same factors that impair proper gating at temperatures above ~200 K (ionic drift, polarization and/or traps) are probably responsible also for the sudden drop in mobility, however, further investigation is required to fully understand charge transport in perovskites.

It was shown that $CH_3NH_3PbI_3$ FETs operating at room temperature, with an ON/OFF ratio of 10^2 and balanced hole and electron mobilities of 1 cm^2/V s, are possible using top-gate structures with Cytop as the gate insulator, as opposed to prior bottom gate devices with silicon oxide as insulator (Fig. 8) [30]. This suggests that traps at the perovskite-insulator interface might be the major factor limiting charge transport in the devices. Moreover the presence of Cytop, a fluorinated polymer, might protect the highly hygroscopic perovskite from moisture, which might also improve performance of the device. Still, the reported stability of the devices was low and subject to fast degradation.

Previously Kagan et al. and Mitzi et al. [23, 24], also reported perovskite FETs working at room temperatures based on tin-based organometallic perovskites, with ON/OFF ratios higher than 10^4. However, tin-based perovskites are known for their relatively low environmental stability. Moreover, the devices reported by Kagan et al. and Mitzi and coworkers seem to work predominately in p-type conduction mode, rather than the ambipolar behavior achieved with $CH_3NH_3PbI_3$. This may be due to the degradation of the Sn-perovskite resulting in high p-type charge carrier density, as discussed in the corresponding section of this chapter.

In spite of the recent advancements in the fabrication of organometallic perovskite FETs, the origin of the very low mobility of these devices compared to the theoretical expectations still needs further clarifications. Several phenomena, such as ionic drift, polarization, and the presence of traps significantly affect charge transport in these materials, which will be discussed next.

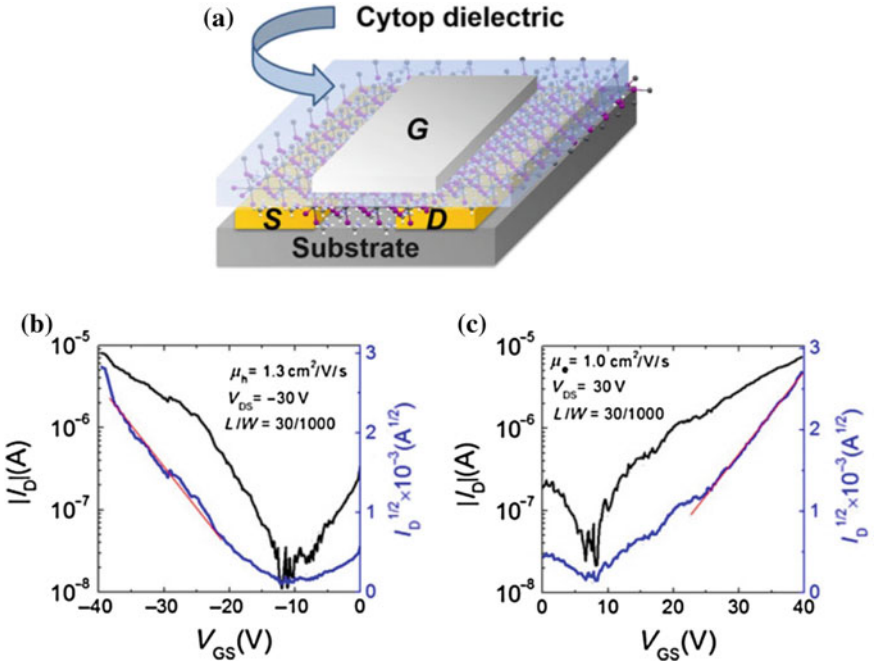

Fig. 8 **a** Schematic structure of the top-gated $CH_3NH_3PbI_{3-x}$ Cl_x FETs having Au source and drain contacts, Cytop gate-dielectric and Al gate electrode. Transfer I–V characteristics for the p-type transport (**b**) and n-type transport (**c**) in $CH_3NH_3PbI_{3-x}$ Cl_x FETs with Cytop gate-dielectric at room temperature. The drain current is plotted versus the gate voltage in *black*, and the square root of the drain current value is plotted in *blue*. The slope used in mobility estimation is shown in *red*. Adapted and printed with permission from [30]

5 The Role of Ion Drift, Polarization, and Traps

One of the most interesting features of organometallic perovskite transport is the anomalous hysteresis observed in IV-curves [31], the cause of which has been tentatively attributed to three effects: ion drift, polarization/ferroelectricity, and the presence of traps. Unraveling these phenomena has strong implications in the understanding of the charge carrier character and the exact transport mechanism in this class of materials. Currently, there is an ongoing debate in the scientific community regarding the importance of these effects, and whether they come to play in the electrical characteristics of hybrid perovskites.

Ion drift can play a dominant role on charge transport properties of $CH_3NH_3PbI_3$ [29]. The reported giant field-switchable photovoltaic effect was best explained by the formation of p–i–n structures induced by ion drift in the perovskite layer. The motion of the ions toward the opposite charged electrodes causes p- and n-type doped regions in the perovskite layer and respective energy band bending, as

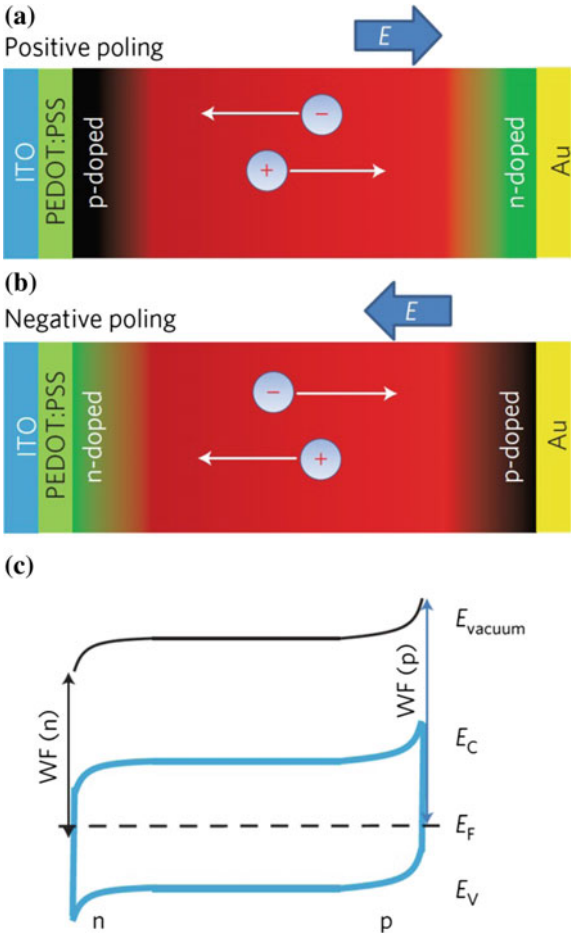

Fig. 9 Schematics of ion drift in perovskite during positive (**a**) and negative poling (**b**), respectively, showing that accumulated ions in the perovskite near the electrodes induced p- and n-doping. **c** Energy diagram of the p–i–n structure after poling (*WF,* workfunction). Adapted and printed with permission from [29]

schematically depicted in Fig. 9. Such self-doping causes a change in the overall resistance and internal electric field of the perovskite layer. Theoretical calculations predicted that negatively charged Pb^{2+} and MA^{+} vacancy could result in p-type doping, whereas positively charged I^{-} vacancy results in n-type doping in $CH_3NH_3PbI_3$ [32, 33]. This behavior was also observed experimentally in composition-dependent studies of $CH_3NH_3PbI_3$, showing evidence of the self-doping of the material [34]. Furthermore, computational modeling of $CH_3NH_3PbI_3$ solar cells shows that the source of the hysteresis is consistent with vacancy assisted migration of iodide ions [35], and the activation energies needed for the ionic drift were found to be in good agreement with experimental kinetic measurements.

On the other hand, ab initio molecular dynamics Monte Carlo simulations [36], indicate that the internal electrical fields associated with microscopic polarization of domains within in $CH_3NH_3PbI_3$ contribute to hysteretic anomalies in hybrid

perovskite devices. The ions present in the perovskite could have high rotational mobility to slowly form ordered polarized domains in response of the applied electric field. The final result is a structured local potential field which is the source of the hysteresis. This polarization hypothesis seems to be corroborated by the different responses of hybrid perovskite devices at different IV-scan rates (Fig. 10) [31], where slower scans, which allow more time for the domain polarization, lead to a higher hysteretic effect.

Investigations of the crystal structure by Stoumpos et al. [9] also noted the possibility for ferroelectric behavior in methylammonium lead iodide and methylammonium tin iodide perovskites. They showed that at room temperature, different possible configurations of the crystal structure of $CH_3NH_3PbI_3$ and $CH_3NH_3SnI_3$ observed by X-ray crystallography are non-centrosymmetric. The space-groups observed are classified in the "ferroelectric distortion" category, where certain symmetries are abolished, including the center of symmetry. This results in the

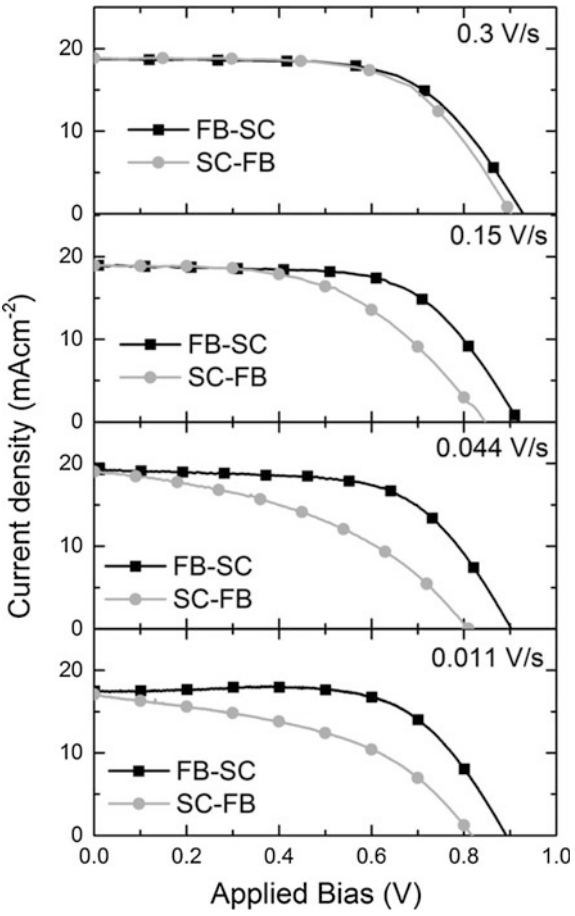

Fig. 10 Influence of scanning conditions on planar heterojunction perovskite solar cell current–voltage characteristics. From forward bias to short circuit (FB-SC, *black*) and from short circuit to forward bias (SC-FB, *gray*) current density–voltage curves for a single solution-processed planar heterojunction perovskite solar cell measured under simulated AM1.5 100 mW cm^{-2} sun light at a range of scan rates from 0.3 to 0.011 V/s. The scans start and finish under forward bias and have 60 s of stabilization time at forward bias (1.4 V) under illumination prior to scanning. Adapted and printed with permission from [31]

displacement of the organic cation from the center of the octahedron in the unit cell. The same experiments note, however, that in addition to ferroelectric distortions also tilting distortions should be taken into consideration.

It has been proposed that the transient processes that occur in IV-characteristics of solar cells are consistent with a polarization response of the $CH_3NH_3PbI_3$ perovskite to the applied electric field [37]. A strong influence of bias preconditioning on IV-measurements seems clear, which could indicate that the internal polarization in the perovskite plays an essential role in the observed current and hysteresis of the device. However, they also notice that the dependence of the hysteretic behavior on bias and light illumination also suggests that photoinduced ion migration might also play an important role in the perovskite transport, especially in regard of slower processes in the device during bias preconditioning.

Finally, it has been demonstrated that by passivating the charge trap states at the interface of the $CH_3NH_3PbI_3$ perovskite by deposition of fullerene layers, the photocurrent hysteresis in perovskite solar cells could be eliminated [38]. Following this approach, the main source of hysteresis in perovskite solar cells would be the trap states at the grain boundaries of the perovskite nanocrystals and the interfaces between the perovskite and the other layers. A schematic depiction of the effect of traps and passivation on charge recombination is shown in Fig. 11. The formation of these traps is explained by the low thermal stability of these materials, which leads to decomposition of the material at higher temperatures (e.g. during annealing), with the introduction of n-doping I-vacancies and compensated by the p-doping in the nondegraded perovskite films. This hysteretic effect is very similar

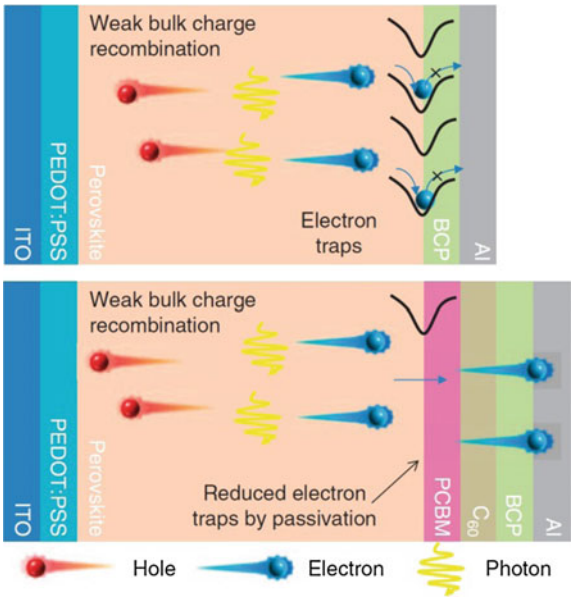

Fig. 11 Schematic depiction of the surface recombination reduction by passivatiing the trap states at the hybrid perovskite interface. Adapted and printed with permission from [38]

to the hysteresis that arises in organic semiconductors with a significant amount of traps [39].

Although different theoretical and experimental results seem to indicate different causes for the hysteresis, there seem to be also correlation between these phenomena. Ionic displacement can be both the source of polarization within a material and also the origin of traps. Polarization can easily induce energetic disorder and broadening of the DoS, hence inducing traps [40]. The debate for the origin, and solution, for the hysteretic behavior in organometallic perovskites is still open, however, the literature here reviewed suggests that more than one single phenomena is at play simultaneously.

6 Polaronic Charge Carriers

The remarkable charge transport features of organometallic halide perovskites discussed above, such as large diffusion length and low recombination rate of the charge carriers, high mobility and low carrier scattering rate [12, 41, 42] seem to suggest that charge carriers originate from scattering with defects, longitudinal optical phonons, and other carriers. Recently, Zhu et al. [43] have proposed that the origin of these remarkable features could be attributed to the polaronic nature of the charge carriers in the hybrid perovskites. The authors hypothesize that a model including the large (delocalized) polarons as charge carriers might explain many of the different peculiar features of metalorganic perovskites. However, the most striking feature is the discrepancy between the very large predicted mobility and the relatively low mobility found in FETs. Although theoretically the effective masses of holes and electrons have been shown to be very small by magneto-absorption measurements [10], there are no reliable measurements of effective carrier mass from transport measurements. However, Zhu et al., note that due to the extremely short lifetimes of the excitons reported in Miyata et al., such absorption measurements only provide information on the nascent electron-hole pairs, before nuclear polarization starts effectively acting on the charge carriers. Hence, the effective masses in the effective transport in diodes, solar cells, and FETs, might be larger than the theoretical expectations, and the currently measured values, and consistent with a large electron–phonon coupling expected in a polaron.

Moreover, the inverse temperature dependence of carrier mobility ($\partial\mu/\partial T < 0$) which has been observed by both spectroscopic [44] and charge transport measurements [4] is consistent with coherent band-like transport of large polarons, where the polaron size and mean-free path is much larger than the lattice constant of the crystal.

Zhu et al. also estimate that the effective mass of electron and holes at room temperature in hybrid perovskites is 100–1000 times larger than the theoretically given values and between 10 m_0 and 300 m_0. Such large values would partially explain the low mobilities in FETs and especially the strong drop in mobility seen above 180 K by [4].

In the case of 2D hybrid perovskites, Cortecchia et al. [59] have shown that the strong charge-phonon coupling resulting from charge confinement in the layered structure causes charge self-localization in specific sites of the inorganic lattice. The resulting strongly localized polarons were found to be responsible for the broad-band light emission observed in various 2D perovskites such as (EDBE) PbX_4 (X = Cl, Br) across the entire visible spectral range, and are thus expected to play a dominant role in the charge transport properties of these materials.

It is important to note that polarons are often the most accurate way to describe electrons and holes within conducting materials, since free charge carriers are usually accompanied by a (local) lattice distortion, coupling phonons, and free electrons or holes [45]. However, the role of polarons in charge transport is dominant only when the electron-phonon coupling becomes sufficiently strong, i.e., in highly polar or ionic conductive solids, [45, 46] such as many II–VI semiconductors and, indeed, (hybrid) perovskites. The cause of the dominant electron/hole-phonon coupling is the stronger Coulomb interaction between a free charge carrier and the lattice ions, compared to less polar materials, such as group IV semiconductors and metals. The stronger coupling leads to a stronger polarization of the lattice, which finally results in an increased effective mass of the charge carrier [47]. Depending on their size, polarons can be classified as either as "small" or "large" [48]. Small polarons are usually involved in hopping transport, such as in organic semiconductors, and have very short diffusion lengths, while large polarons exhibit band-like transport and have very long diffusion lengths, such as the diffusion lengths observed in hybrid perovskites. This is very consistent with the model provided by Zhu et al. and with the relatively low charge carrier mobilities measured in FETs. In conclusion, along with ionic drift, ferroelectric polarization and traps, dominant polaronic charge transport might be one of the main causes of the discrepancy between the theorized high mobilities and the much lower mobilities observed in FETs.

7 Transport in Emerging Perovskite Materials

In spite of the many new advances, organometallic halide perovskites remain a relatively new field in material science, and the main focus of past investigations, with some exceptions, has been mainly aimed at bulk lead-based perovskites. However, recently two particular classes of hybrid perovskites are becoming the target of research. The first class is 2D hybrid perovskites. These materials, unlike graphene or other conventional 2D systems, can be grown from solution, with the possibility to form both 2D-layered structures, such as $(C_6H_5C_2H_4NH_3)2SnI_4$ [23] or even monoatomically thin sheets [49]. Low-dimensional systems offer new interesting challenges and open the possibility to new physical features, also regarding charge transport, thus 2D perovskites are currently gaining attention in the field. The second class of materials is lead-free organometal halide perovskites, which target one of the main concerns in current hybrid perovskite technology: the

presence of lead in the devices. Concerns due to the toxicity of lead may limit widespread implementation of lead-based solar cells and light-emitting devices. Although proper encapsulation and disposal of lead-based devices might minimize any possible risks, this will also increase the costs involved in the production of solar panels or LEDs. These challenges have resulted in increased emphasis on the research of lead-free perovskite materials.

The concept of lower dimensionality (<3D) perovskites lies in the distance between the material layers. The separation of some of these layers in the 3D structure can be achieved, for instance, by the substitution of the cation in the "A" position by a larger sized counterpart (see Fig. 12). The reduction of the stacked layers between the larger cation layers decreases the dimensionality of the material, reaching a typical 2D perovskite when there is a single inorganic layer between the large (organic) cationic layer. Theoretical investigations of 2D organometallic perovskites [50] predict a band structure with very low dispersion in the direction of reciprocal space corresponding to the stacking axis of the layers. Theoretical calculations also show that while the Wannier excitons in 3D hybrid perovskites is strongly screened by collective molecular rotations and vibrations of the inorganic

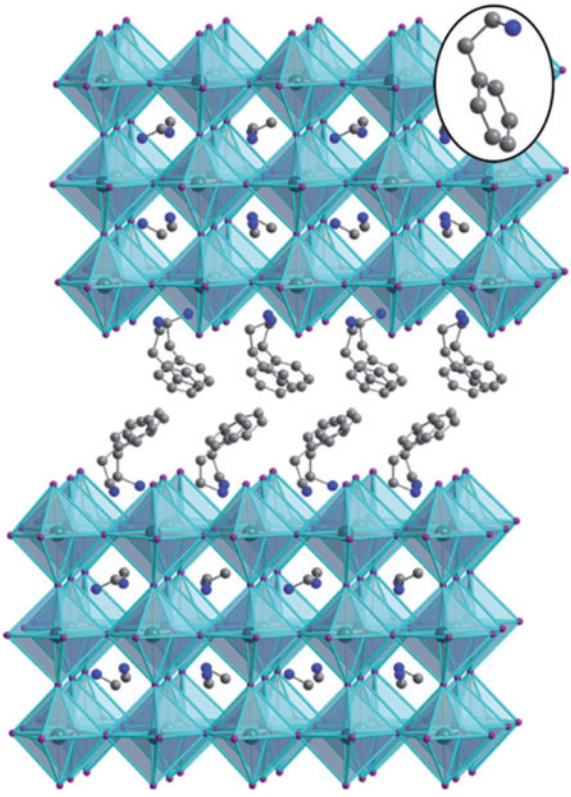

Fig. 12 Schematic representation of a 2D-layered hybrid perovskite. The perovskite had a layered structure, with a few monolayers of perovskite 2D-crystals stacked upon each other and separated by a spacer constituted by an organic molecule bilayer. Adapted and printed with permission from [51]

lattice, this screening does not occur in 2D perovskites [61]. Moreover, a larger bandgap and stronger exciton binding energy is predicted as well.

Experimentally [51], solution-processed 2D-layered perovskites have been achieved. It has been shown that decreasing the dimensionality of the inorganic components, from a 3D- to a 2D-layered structure induces an increase in the bandgap of the perovskite and an increase in the exciton binding energy, which confirms the theoretical predictions.

Despite the increase in exciton binding energy, which can reach up to several 100 meV, the delocalization of the exciton wave function still covers several unit cells in the layer plane, hence it does not have to fully sacrifice the large diffusion lengths that have been observed in 3D perovskites [52].

Recently [49], atomically thin $(C_4H_9NH_3)_2PbBr_4$ 2D perovskites crystals have also been fabricated by solution-phase growth. These 2D structures, only a few monolayers thick, exhibit efficient photoluminescence (Fig. 13), and enable tuning the emission spectrum by changing either the thickness or the chemical composition of the perovskite itself. An exfoliation process can be used for the fabrication of similar 2D perovskites as well [53].

An interesting advantage of the increased bandgap predicted and observed in 2D hybrid perovskites is the possibility for white-light emission. Dohner et al. [54] reported white-light emitting *N*-methylethane-1,2-diammonium lead halide (with a bromine and chloride mixture) 2D perovskites. The observed photoluminescence intensity increases linearly with UV-excitation power density with no signs of saturation, indicating that white-light emission does not depend on the presence of traps within the material, but it is rather a bulk property of the 2D-layered structure of the perovskite.

As previously discussed, Kagan et al., showed tin-based 2D-layered hybrid perovskites in FETs, showing good gating characteristics and mobility even at room temperature. In parallel, 2D-layered perovskite solar cells also showed higher V_{OC} and higher stability to moisture and environmental stability, which is very important for commercialization.

In conclusion, 2D hybrid perovskite structures offer new possibilities for different applications: both in more stable photovoltaic devices, FETs, and electroluminescence applications.

Currently, a few alternatives to lead as the metal cation in hybrid perovskites have already been offered. Several investigations [55–57] have shown promising results in solar cells with tin-based methylammonium halide perovskites, reaching efficiencies up to 5.73 %, in addition to the mentioned tin-based perovskites in FETs. However, tin-based perovskites are very unstable mainly due to p-type doping via Sn^{2+} oxidation, especially when exposed to environmental conditions, leading to very short lifetime of the devices. This has strong implications in the charge transport properties of these materials, going from an almost intrinsic semiconductor model (the case of $CH_3NH_3PbI_3$), to a heavily p-doped one (Sn-based perovskites).

Copper-based organometallic perovskites were investigated from a crystallographic point of view more than 20 years ago [58], mainly in the field of magnetic

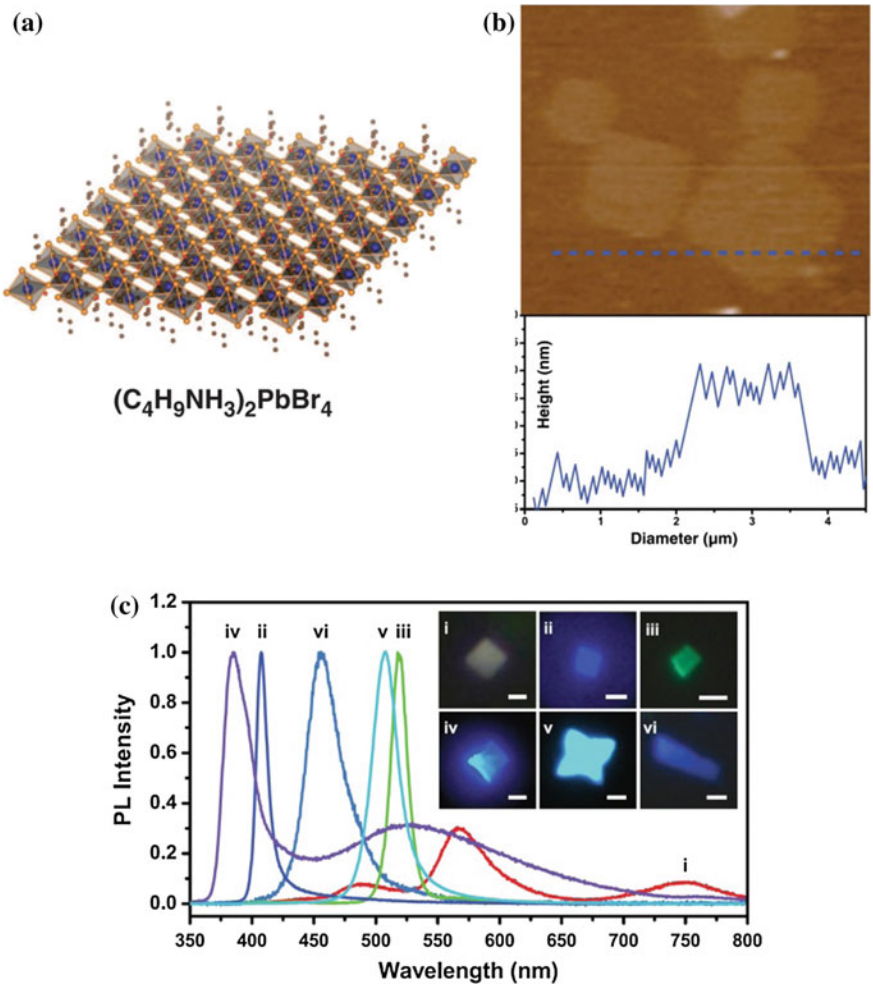

Fig. 13 **a** Structural illustration of a single layer $(C_4H_9NH_3)_2PbBr_4$. **b** AFM image and height profile of several single layers. The thickness is around 1.6 nm (±0.2 nm). **c** Photoluminescence of different 2D hybrid perovskites. $(C_4H_9NH_3)_2PbCl_4$ (*i*), $(C_4H_9NH_3)_2PbBr_4$ (*ii*), $(C_4H_9NH_3)_2PbI_4$ (*iii*), $(C_4H_9NH_3)_2PbCl_2Br_2$ (*iv*), $(C_4H_9NH_3)_2PbbBr_2I_2$ (*v*), and $(C_4H_9NH_3)_2(CH_3NH_3)Pb_2Br_7$ (*vi*) 2D sheets demonstrate that the solution-phase direct growth method is generalizable. The corresponding optical PL images are shown in the inset. Scale bars, 2 mm for (*i*)–(*v*) and 10 mm for (*vi*). Adapted and printed with permission from [49]

materials. Most studies conducted so far have dealt with the synthesis of stable copper-based perovskites, however, no copper-based perovskite device had been reported in the literature until recently, when the first application of copper-based hybrid perovskites $(CH_3NH_3)_2CuCl_xBr_{4-x}$ as light harvester in solar cells was showed [59]. The strong charge transport anisotropy in these layered copper perovskites,

combined with the low absorption coefficient and high hole effective mass, strongly limit the device efficiency. The incorporation of optoelectronically active organic cations in the perovskite scaffold should be used to improve the performance.

Germanium-based lead-free perovskites with promising characteristics for photovoltaic applications [60] have also recently been reported.

In conclusion, despite the progress made toward lead-free efficient hybrid perovskite devices, only the tin-based alternatives have shown some promising results.

Several problems related to the charge transport are hindering the full expansion of 2D and lead-free perovskites. The anisotropy of the charge transport in the low dimensionality perovskites and the strong p-doping in the tin-based ones are clear examples of this. Thus, the full understanding and control of the electrical properties will be a key aspect in the search for 2D and lead-free alternatives. Much theoretical and experimental work still needs to be done to obtain materials with performance comparable to lead-based perovskites.

8 Summary and Conclusions

The field of organometal halide perovskites has shown great progress in the past 5 years, both regarding technological applications and fundamental studies of this relatively new class of materials. This chapter has focused on the charge carrier transport and behavior of this kind of materials. Theoretical investigations have shown results that indicate the characteristic of hybrid perovskites are in many aspects similar to those of crystalline semiconductors, such as low effective mass of the charge carriers, long diffusion lengths, and mobilities in the order of thousands $cm^2\ V^{-1}\ s^{-1}$. Several of these results have also been experimentally confirmed, such as high Hall-effect mobilities and diffusion lengths of charge carriers in the order of hundred micrometers. However, the effective mobilities in devices such as field-effect transistors are much lower than the theoretically predicted values and the values measured by techniques such as Hall-effect, being in the order of $1\ cm^2\ V^{-1}\ s^{-1}$ or less. The discrepancy in the theoretical and effective mobility and the presence of a strong hysteretic behavior in hybrid perovskite devices had given rise to several theories to explain the presence of these anomalies. The possibility of ionic drift, ferroelectric polarization, and trap-states has been thoroughly investigated in the past few years. Although no consensus has been reached yet, it is probable that more than one or even all of these phenomena play a role in charge transport in hybrid perovskites. Recent data has also indicated the possibility that the nature of the charge carrier in hybrid perovskites is polaronic in nature, with higher effective masses than theoretically predicted, which might also explain the lower than expected mobility. Finally, we have also looked at transport in emerging perovskite materials: 2D (layered) perovskites and lead-free perovskites for environmentally-friendly applications. The astounding progress with $CH_3NH_3PbI_3$ solar cells has created a new urgency for the study of organometallic halide perovskites. However, many questions are yet to be fully unanswered and new

developments and applications would undoubtedly stem from the improved understanding of the charge transport phenomena in these multidimensional perovskites.

References

1. Shen, Q., et al.: J. Mater. Chem. A **3**, 9308–9316 (2015)
2. Xing, G., et al.: Nat. Mater. **13**, 476–480 (2014)
3. Tan, Z.-K., et al.: Nat. Nanotechnol. **9**, 687–692 (2014)
4. Chin, X.Y., et al.: Nat. Comm. **6**, 7383 (2015)
5. He, Y., Galli, G.: Chem. Mater. **26**, 5394–5400 (2014)
6. Brivio, F., et al.: APL Mater. **1**, 042111 (2013)
7. Brivio, F., et al.: Phys. Rev. B **89**, 155204 (2014)
8. Eperon, et al.: Energy Environ. Sci. **7**, 982 (2014)
9. Stoumpos, et al.: Inorg. Chem. **52**, 9019–9038 (2013)
10. Miyata, et al.: Nat. Phys. **11**, 582–587 (2015)
11. Stranks, et al.: Science **342**, 341–344 (2013)
12. Xing, et al.: Science **342**, 344–347 (2013)
13. Giorgi, et al.: J. Phys. Chem. Lett. **4**, 4213–4216 (2013)
14. Dong, et al.: Science **347**, 967–970 (2015)
15. Chung, et al.: J. Am. Chem. Soc. **134**, 8579 (2012)
16. Castelli, et al.: APL Mater. **2**, 081514 (2014)
17. Papavassiliou and Koutselas: Synth. Met. **71**, 1713 (1995)
18. Beaujuge, et al.: J. Am. Chem. Soc. **133**, 20009–20029 (2011)
19. Facchetti, Chem: Mater. **23**, 733–758 (2011)
20. Selinsky, et al.: Chem. Soc. Rev. **42**, 2963–2985 (2013)
21. Dharani, et al.: Nanoscale **6**, 13854–13860 (2014)
22. Yantara, et al.: Chem. Mater. **27**, 2309–2314 (2015)
23. Kagan, et al.: Science **286**, 945 (1999)
24. Mitzi, et al.: Chem. Mater. **13**, 3728–3740 (2001)
25. Mitzi, et al.: Adv. Mater. **14**, 1772–1776 (2002)
26. Li, et al.: Nat. Comm. **6**, 8238 (2015)
27. Luzo, et al.: Sci. Rep. **3**, 3425 (2013)
28. McCulloch, et al.: Nat. Mater. **5**, 328–333 (2006)
29. Xiao, et al.: Nat. Mater. **14**, 193–198 (2015)
30. Mei, et al.: MRS Commun. **5**, 297–301 (2015)
31. Snaith, et al.: J. Phys. Chem. Lett. **5**, 1511–1515 (2014)
32. Yin, et al.: Appl. Phys. Lett. **104**, 063903 (2014)
33. Kim, et al.: J. Phys. Chem. Lett. **5**, 1312–1317 (2014)
34. Wang, et al.: Appl. Phys. Lett. **105**, 163508 (2014)
35. Eames, et al.: Nat. Comm. **6**, 7497 (2015)
36. Frost, et al.: APL Mater. **2**, 081506 (2014)
37. Unger, et al.: Energy Environ. Sci. **7**, 3690–3698 (2014)
38. Shao, et al.: Nat. Comm. **5**, 5784 (2014)
39. Lindner, et al.: J. Appl. Phys. **98**, 114505 (2005)
40. Richards, et al.: J. Chem. Phys. **128**, 234905 (2008)
41. Trinnh, et al.: J. Mater. Chem. A **3**, 9285–9290 (2015)
42. Price, et al.: Nat. Comm. **6**, 8420 (2015)
43. Zhu and Podzorov: J. Phys. Chem. Lett. **6**, 4758–4761 (2015)
44. Milot, et al.: Adv. Funct. Mater. **25**, 6218–6227 (2015)

45. Devreese, Encycl: Appl. Phys. **14**, 383–409 (1996)
46. Grundmann, M.: The Physics of Semiconductors; An Introduction Including Nanophysics and Applications. Springer (2010)
47. Emin, D.: Polarons. Cambridge University Press, Cambridge (2013)
48. Appel: Solid State Phys. **21**, 193–391 (1968)
49. Dou, et al.: Science **349**, 1518–1521 (2015)
50. Pedesseau, et al.: Opt. Quant. Electron. **46**, 1225–1232 (2014)
51. Smith, et al.: Angew. Chem. Int. Ed. **53**, 11232–11235 (2014)
52. Lanty, et al.: J. Phys. Chem. Lett. **5**, 3958–3963 (2014)
53. Niu, et al.: Appl. Phys. Lett. **104**, 171111 (2014)
54. Dohner, et al.: J. Am. Chem. Soc. **136**(38), 13154–13157 (2014)
55. Hao, et al.: Nat. Photonics **8**, 489–494 (2014)
56. Kumar, et al.: Adv. Mater. **26**, 7122 (2014)
57. Noel, et al.: Energy Environ. Sci. **7**, 3061–3068 (2014)
58. Willett, et al.: J. Am. Chem. Soc. **110**, 8639–8650 (1988)
59. Cortecchia, et al.: Inorg. Chem. (accepted manuscript) (2016)
60. Krishnamoorthy, et al.: J. Mater. Chem. A (accepted manuscript) (2016)
61. Even, et al.: J. Phys. Chem. C 119, 10161–10177 (2015)